CellPress
PARTNER JOURNAL

Molecular Plant
Research Article

Histone Deacetylase HDA9 and WRKY53 Transcription Factor Are Mutual Antagonists in Regulation of Plant Stress Response

Yu Zheng[1,3,*], Jingyu Ge[1,3], Chun Bao[1], Wenwen Chang[1], Jingjing Liu[1], Jingjie Shao[1], Xiaoyun Liu[1], Lufang Su[1], Lei Pan[1] and Dao-Xiu Zhou[2,*]

[1]Institute for Interdisciplinary Research and Hubei Province Engineering Research Center of Legume Plants, Jianghan University, Wuhan 430056, China

[2]Institute of Plant Sciences Paris-Saclay, CNRS, INRAE, Université Paris-Saclay, Orsay 91405, France

[3]These author contributed equally to this article.

***Correspondence: Yu Zheng (zhengyu320@126.com), Dao-Xiu Zhou (dao-xiu.zhou@u-psud.fr)**

https://doi.org/10.1016/j.molp.2019.12.011

ABSTRACT

Epigenetic regulation of gene expression is important for plant adaptation to environmental changes. Previous results showed that Arabidopsis RPD3-like histone deacetylase HDA9 is known to function in repressing plant response to stress in *Arabidopsis*. However, how HDA9 targets to specific chromatin loci and controls gene expression networks involved in plant response to stress remains largely unclear. Here, we show that HDA9 represses stress tolerance response by interacting with and regulating the DNA binding and transcriptional activity of WRKY53, which functions as a high-hierarchy positive regulator of stress response. We found that WRKY53 is post-translationally modified by lysine acetylation at multiple sites, some of which are removed by HDA9, resulting in inhibition of WRKY53 transcription activity. Conversely, WRKY53 negatively regulates HDA9 histone deacetylase activity. Collectively, our results indicate that HDA9 and WRK53 are reciprocal negative regulators of each other's activities, illustrating how the functional interplay between a chromatin regulator and a transcription factor regulates stress tolerance in plants.

Key words: HDA9, WRKY53, stress, lysine acetylation, transcription activity

Zheng Y., Ge J., Bao C., Chang W., Liu J., Shao J., Liu X., Su L., Pan L., and Zhou D.-X. (2020). Histone Deacetylase HDA9 and WRKY53 Transcription Factor Are Mutual Antagonists in Regulation of Plant Stress Response. Mol. Plant. **13**, 598–611.

INTRODUCTION

Salt-triggered abiotic stress is one of the most common environmental stresses endured by plants and exerts evolutionary pressure on plants, which, in turn, have developed sophisticated responses to cope and to survive (Zhu, 2002). Thus, knowledge of the mechanisms underlying the response to salt stress has profound implications in many biotechnological applications, including increasing plant productivity and protecting the environment. Regulation of response to salt stress is a complex process controlled by developmental and environmental signaling pathways (Ingram and Bartels, 1996; Xiong et al., 2002; Shinozaki et al., 2003; Bohnert et al., 2006; Jeandroz and Lamotte, 2017). Recent results have shown that histone acetylation/deacetylation is an essential process in the epigenetic regulation of gene expression involved in plant response to environmental changes and stress (Kawashima and Berger, 2014; Liu et al., 2015; Shen et al., 2015). The dynamic equilibrium between histone acetyltransferases and histone deacetylases (HDACs) controls histone acetylation levels of nucleosomes, affecting chromatin structure and gene activity (Mikkelsen et al., 2007). Histone acetyltransferases promote gene transcription, while HDACs are generally associated with transcriptional repression and gene silencing (Verdin and Ott, 2015).

HDACs are highly conserved enzymes in eukaryotes. In *Arabidopsis*, 18 HDACs have been identified, of which 12 belong to the reduced potassium dependency 3 (RPD3/HDA1) subfamily, four to the HDAC2 subfamily, and two to the silent information regulator 2 or sirtuin subfamily (Pandey et al., 2002; Alinsug et al., 2009). Many *Arabidopsis* HDACs have been shown to be

Published by the Molecular Plant Shanghai Editorial Office in association with Cell Press, an imprint of Elsevier Inc., on behalf of CSPB and IPPE, CAS.

involved in plant response to stress. For instance, several members of the RPD3/HDA1 subfamily, including HDA6, HDA9, and HDA19, function in plant stress response by regulating gene expression through histone deacetylation (Chen et al., 2010; Chen and Wu, 2010; Zheng et al., 2016; Kim et al., 2017; Luo et al., 2017; Hu et al., 2019; Shen et al., 2019). Although the mechanism by which HDACs target to specific loci is generally unclear, HDA19 was shown to form transcriptional repressor complexes with other proteins to regulate plant response to abiotic stress through histone deacetylation at specific target genes (Song et al., 2005; Wang et al., 2013).

HDA9 has been shown to regulate histone acetylation and expression of genes involved in different biological processes, including flowering time, seed germination, stress resistance, and senescence. For example, HDA9 deacetylates H3K9 and H3K27 in the promoter of *AGL19*, a flowering-promoting gene, and represses its expression and flowering (Kim et al., 2013, 2016; Kang et al., 2015). In addition, HDA9-mediated histone deacetylation suppresses the expression of key negative regulators of senescence genes, which in turn induces the derepression of their downstream genes to promote leaf senescence (Chen et al., 2016; Kim et al., 2016). Furthermore, HDA9-mediated histone deacetylation represses genes involved in photo-autotrophy and photosynthesis and thus inhibits seed germination (Zanten et al., 2014). It was shown that HDA9 loss of function resulted in a more stress-resistant phenotype, and that HDA9 regulates histone acetylation levels of a large number of stress-responsive genes to negatively regulate plant sensitivity to salt and drought stresses (Zheng et al., 2016). These results indicate that HDA9 is a potent epigenetic regulator of histone acetylation and expression of genes involved in both developmental and stress-responsive pathways. Unlike other HDACs that play positive roles in plant response to stress, HDA9 appears to be a negative regulator of plant tolerance to stress. However, the underlying mechanism by which HDA9 represses plant stress tolerance response is unclear. Recent results from proteomic screening revealed that HDA9 interacts with transcription factors such as the MYB protein POWERDRESS and WRKY53 (Chen et al., 2016). Interaction between HDA9 and POWERDRESS is shown to promote senescence in *Arabidopsis* (Chen et al., 2016). WRKY53 was previously reported to play a central role in stress response and during the early events of leaf senescence (Miao et al., 2007; Miao and Zentgraf, 2007; Murray et al., 2007; Zentgraf et al., 2010; Sarwat, 2017; Chen et al., 2019). The functional significance of the interaction between HDA9 and WRKY53 is unclear.

In this work, we identified domains within the WRKY53 and HDA9 proteins involved in their interaction and studied their functional relationship and reciprocal regulation in controlling gene expression and plant tolerance to salt stress. We show that *wrky53* loss-of-function mutants and HDA9-overexpressing (OE) plants display higher sensitivity to salt stress. Conversely, *hda9* loss-of-function mutants and WRKY53-OE plants are more resistant to salt stress. Importantly, we demonstrate that WRKY53 is post-translationally modified by lysine acetylation and that HDA9 represses the transcription activity of WRKY53 by mediating its lysine deacetylation. Our data suggest that the deacetylase activity of HDA9 could be inhibited by WRKY53 interaction, uncovering a novel mechanism underlying plant response to stress that illustrates how the interaction between an HDAC and a transcription factorfunctions in the regulation of plant stress tolerance.

RESULTS

The HDA9 Deacetylase Domain Interacts with the WRKY53 DNA-Binding Domain

Previous results showed interaction between HDA9 and WRKY53 (AT4G23810) in yeast two-hybrid (Y2H) assays (Chen et al., 2016). We confirmed the interaction in Y2H assays and in bimolecular fluorescence complementation (BiFC) assays in *Arabidopsis* leaf protoplasts (Figure 1A and 1B). To further study the *in vivo* interaction between HDA9 and WRKY53, we performed co-immunoprecipitation (Co-IP) assays with transgenic *Arabidopsis* plants expressing GFP-tagged WRKY53 (WRKY53-OE, Supplemental Figure 1) using anti-GFP and anti-HDA9 antibodies (Supplemental Figure 2). The HDA9 protein could be precipitated by anti-GFP, and the WRKY53-GFP fusion could be precipitated by anti-HDA9 (Figure 1C). To identify interacting domains, we truncated both HDA9 and WRKY53 into three segments and tested the pairwise combinatorial interactions between the segments in Y2H assays. The analysis revealed that the central deacetylase domain of HDA9 interacted with the DNA-binding domain of WRKY53 (Figure 1D). The HDA9 and WRKY53 interaction appeared to be specific, as no interaction was detected between WRKY53 and other HDACs (i.e., HDA6, HDA9, HDA19, and SRT1) or between HDA9 and other WRKY proteins (i.e., WRKY22, WRKY38, WRKY53, and WRKY62) in Y2H assays (Supplemental Figure 3).

WRKY53 and HDA9 Have Opposite Functions in Regulating Plant Response to Salt Stress

We have shown that HDA9 plays a negative role in regulating plant sensitivity to salt and drought stresses (Zheng et al., 2016). To study the functional relationship between HDA9 and WRKY53, we produced HDA9-OE (oe9-2 and oe9-3) and WRKY53-OE (oe53-wt-1 and oe53-wt-2) lines and characterized two transfer-DNA (T-DNA) insertion lines of *WRKY53* (*wrky53-1* and *wrky53-2*) (Supplemental Figure 1). These lines, together with the *hda9-1* and *hda9-2* mutants (Kim et al., 2013) and the wild type (Col-0), were tested for germination rates on normal Murashige–Skoog (MS) medium and MS supplemented with NaCl (100 mM), polyethylene glycol (PEG) (−0.75 MPa), or mannitol (150 mM). The germination rates were scored 78 h after sowing. Seeds from three different harvests were tested. Under normal conditions, the germination rates of wild type, mutants, and the transgenic lines were more than 90% (Figure 2A). When treated with NaCl, PEG, or mannitol, the germination rates of *wrky53* and HDA9-OE seeds were lower (7.36%–12.27%) than those of wild type (14.11%–18.89%, $p < 0.05$). Conversely, the germination rates of *hda9*-1 and WRKY53-OE seeds were much higher (35.30%–47.48%) than those of wild type ($p < 0.05$, Figure 2A). The data indicated that mutation or overexpression of WRKY53 and HDA9 had opposite effects on seed germination sensitivity to the tested stresses.

To study the effects of overexpression and mutation of *HDA9* and *WRKY53* on stress resistance, we tested seedling growth of the

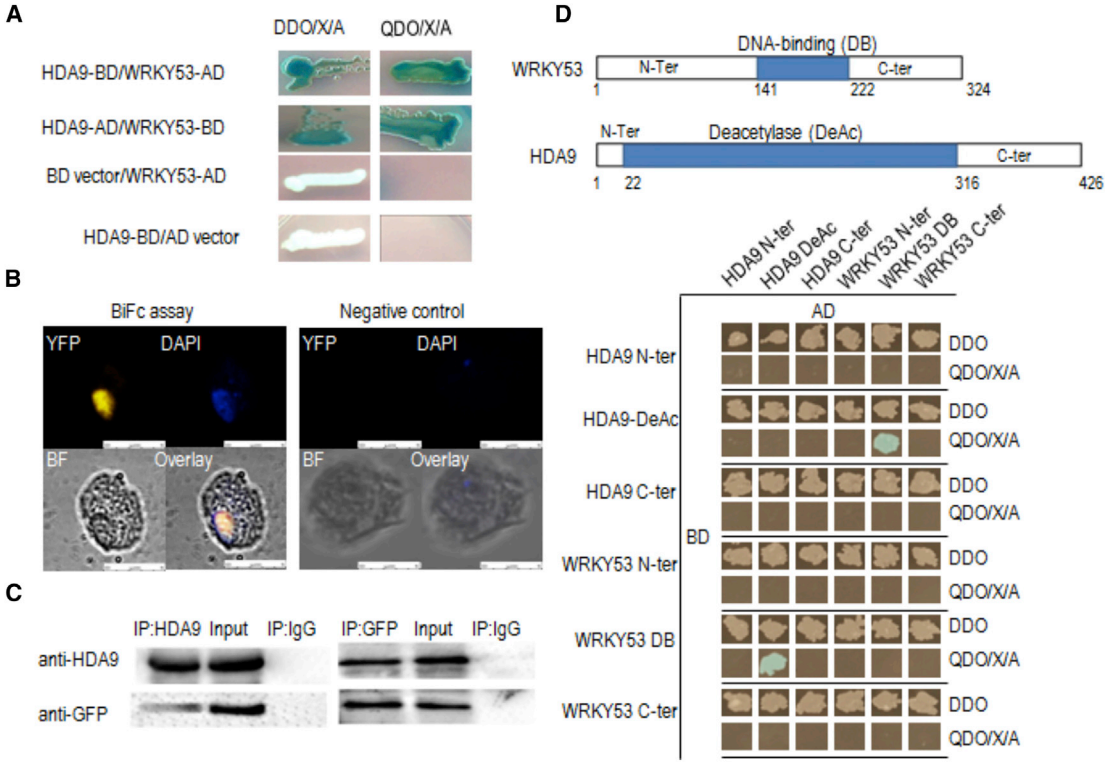

Figure 1. The HDA9 Deacetylase Domain Interacts with the DNA-Binding Domain of WRKY53.

(A) Yeast two-hybrid analysis of interaction between HDA9 and WRKY53. Yeast Gold cells were co-transformed with a combination of the indicated plasmids. Yeast cells were plated on selective medium, DDO/X/A or QDO/X/A, and then incubated for 5 days. DDO/X/A means double-dropout medium: SD/−Leu/−Trp supplemented with X-α-Gal and aureobasidin A. QDO/X/A means quadruple-dropout medium: SD/−Ade/−His/−Leu/−Trp supplemented with X-α-Gal and aureobasidin A.

(B) BiFC analysis of HDA9 and WRKY53 interaction. *p*HDA9-YFPC and *p*WRKY53-YFPN were co-transformed into *Arabidopsis* protoplasts. The empty *p*YFPC and *p*WRKY53-YFPN vectors were co-transformed as the negative control. DAPI staining was used to visualize nuclei. Images were obtained using a confocal microscope (Leica DM IRE2).

(C) Co-IP assays of HDA9 and WRKY53 interaction *in vivo*. Total proteins extracted from WRKY53-GFP transgenic plants were incubated with or without (input) protein A beads and anti-GFP or anti-HDA9. The total proteins and the eluate from the agarose resin were analyzed by immunoblotting with anti-GFP and anti-HDA9 antibodies using the ECL SuperSignal system.

(D) The coding regions of HDA9 and WRKY53 were divided into three parts (top), fused with the GAL4-AD and -BD domains, and tested in pairwise combinations to test interaction in a yeast two-hybrid assay as in **(A)**.

wild type, mutants, and OE plants in soil in the presence of 100 mM NaCl for 30 days. Compared with wild type, *hda9* (*hda9-1*, *hda9-2*) and WRKY53-OE (oe53-wt-1, oe53-wt-2) plants were more resistant, while the *wrky53* (*wrky53-1*, *wrky53-2*) and HDA9-OE (oe9-2, oe9-3) plants were more sensitive to the salt stress (Figure 2B and Supplemental Figure 4A). Under 100 mM NaCl, the abscisic acid (ABA) contents of *wrky53* and HDA9-OE plants were also significantly lower ($p < 0.05$), whereas that of *hda9* was much higher ($p < 0.05$) than that of the wild type. WRKY53-OE lines had a similar ABA content compared with wild type (Figure 2C). We also tested fresh water loss rates of leaves detached from plants of the different genotypes over 6.5 h. At all of the tested time points the fresh water loss rate of *wrky53* was higher, whereas those of *hda9* and WRKY53-OE plants were lower than that of the wild type. The fresh water loss rate of HDA9-OE lines was lower than that of the wild type in the first 2 h, but subsequently increased and was higher than that of wild type (Figure 2D). Thus, the ranking of genotypes based on fresh water loss rate was as follows: *wrky53* > HDA9-OE > wild type > WRKY53-OE > *hda9*.

To further test WRKY53 function in stress response, we transformed *35S:WRKY53-GFP* into different genetic backgrounds (Supplemental Figure 1). In the *wrky53-1* background, *35S:WRKY53-GFP* likely complemented the mutation, as the plant displayed a similar phenotype compared with wild type under NaCl stress (Supplemental Figure 4B). In the *hda9-1* and HDA9-OE (oe9-2) backgrounds, *35S:WRKY53-GFP* transgenic lines showed similar phenotypes compared with *hda9-1* and HDA9-OE (oe9-2), respectively, under both control and stress conditions (Figure 2B and Supplemental Figure 4B). The results indicated that *HDA9* and *WRKY53* have opposite functions in plant response to abiotic stress, with *HDA9* being a negative regulator and *WRKY53* a positive regulator.

HDA9 Represses Expression of *WRKY53* and Its Downstream Targets

Our data are in line with previous results showing that *WRKY53* plays a critical role in regulating responses to diverse stresses, including drought, ozone, hydrogen peroxide, and salicylic

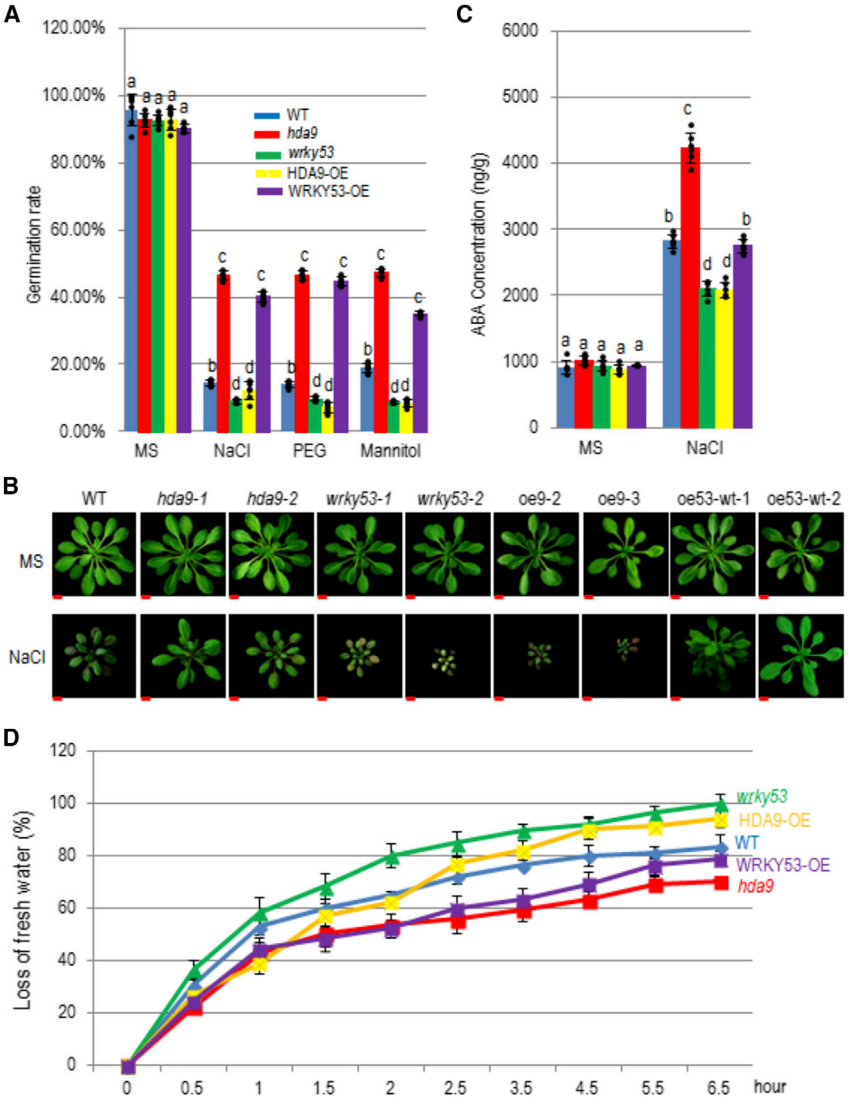

Figure 2. WRKY53 and HDA9 Have Opposite Functions in the Regulation of Response to Salt Stress.

(A) Seed germination rates of the different genotypes under NaCl (100 mM), PEG (−0.75 MPa), and mannitol (150 mM) treatments. Seeds (100 seeds per genotype per treatment) were grown on stress medium. Germination (fully emerged radicle) was scored after 78 h. Seeds grown on 1/2MS were used as a control. Two mutant alleles of *hda9* (*hda9*-1 and *hda9*-2) and *wrky53* (*wrky53-1* and *wrky53-2*) and two lines of HDA9-OE (oe9-2 and oe9-3) and WRKY53-OE (oe53-wt1 and oe53-wt2) were tested with three biological replicates for each line. Bars represent means ± SE with six (3 × 2 lines) biological replicates, and multiple comparison tests (Fisher's LSD) were conducted to analyze significant differences among samples. Different letters represent significant differences between samples.
(B) Plant phenotypes of the different genotypes under NaCl (100 mM) treatment. Seeds were sown on 1/2MS medium to obtain uniform germination, and after 4 days seedlings were transferred to soil and grown for 30 days with and without NaCl treatment before taking photographs. Bar, 0.5 cm.
(C) ABA contents of the different genotypes under 100 mM NaCl treatment. ABA contents in two whole seedlings per genotype were determined by ELISA. Bars represent means ± SE from six (3 × 2 lines) biological replicates, and multiple comparison tests (Fisher's LSD) were conducted to analyze significant differences among samples. Different letters represent significant differences between samples.
(D) Water loss rates of the different genotypes. The sixth rosette leaf was excised at the same developmental stage (early senescence phase, approximately 25% yellowing) and exposed to light (110 μmol m^{-2} s^{-1}) at 22°C. Six plants per genotype were used for the analysis. Leaves were weighed at various time points, and the loss of fresh weight (%) was used to represent the water loss rate. The same lines as those used in **(A)** and **(C)** were tested. Bars represent means ± SE from six (3 × 2 lines) biological replicates, and multiple comparison tests (Fisher's LSD) were conducted to analyze significant differences among samples.

acid, as well as pathogen infection (Miao et al., 2007; Miao and Zentgraf, 2007; Murray et al., 2007; Zentgraf et al., 2010; Sarwat, 2017). *WRKY53* expression is also induced by drought stress (Sun and Yu, 2015). The physical association between WRKY53 and HDA9 and their apparently opposite functions in stress response suggested that the two proteins may antagonistically regulate stress-responsive gene expression. Therefore, we tested whether *HDA9* regulates *WRKY53* expression by analyzing *WRKY53* transcript levels in wild type, *hda9-1*, and HDA9-OE (oe9-2) plants. Under normal conditions, the *WRKY53* transcript level was significantly higher ($p < 0.05$, >two-fold) in *hda9-1* and lower ($p < 0.05$, >two-fold) in HDA9-OE than in wild type. Under salt stress, the level of *WRKY53* expression was not clearly changed in wild-type plants, but induced in *hda9-1* ($p < 0.05$, >two-fold) mutant plants (Figure 3). In HDA9-OE plants, the NaCl treatment increased *WRKY53* expression only to the wild-type level. The data suggested that HDA9 represses *WRKY53* expression under normal conditions and inhibits induction of the gene under salt stress. Interestingly, salt stress further increased *WRKY53* expression in the WRKY53-OE plants. A possible explanation is that WRK53-OE overcame the inhibitory effect of HDA9 on salt-stress induction of *WRKY53* (see below). *WRKY53* expression levels in the different genotypes correlated with the level of plant resistance to 100 mM NaCl (Figure 2), indicating that WRKY53 expression level is an important factor in conferring plant resistance to the stress, which is negatively regulated by HDA9.

In addition to its autoactivation, *WRKY53* was shown to also regulate other WRKY family members (Miao et al., 2004). Under normal conditions, *WRKY13*, *WRKY15*, *WRKY18*, *WRKY22*, *WRKY29*, and *WRKY62* are activated by WRKY53, whereas *WRKY6* and *WRKY42* are negatively regulated by WRKY53 (Miao et al., 2004). Therefore, we examined the expression of these WRKY genes in different *HDA9* and *WRKY53* genotypes

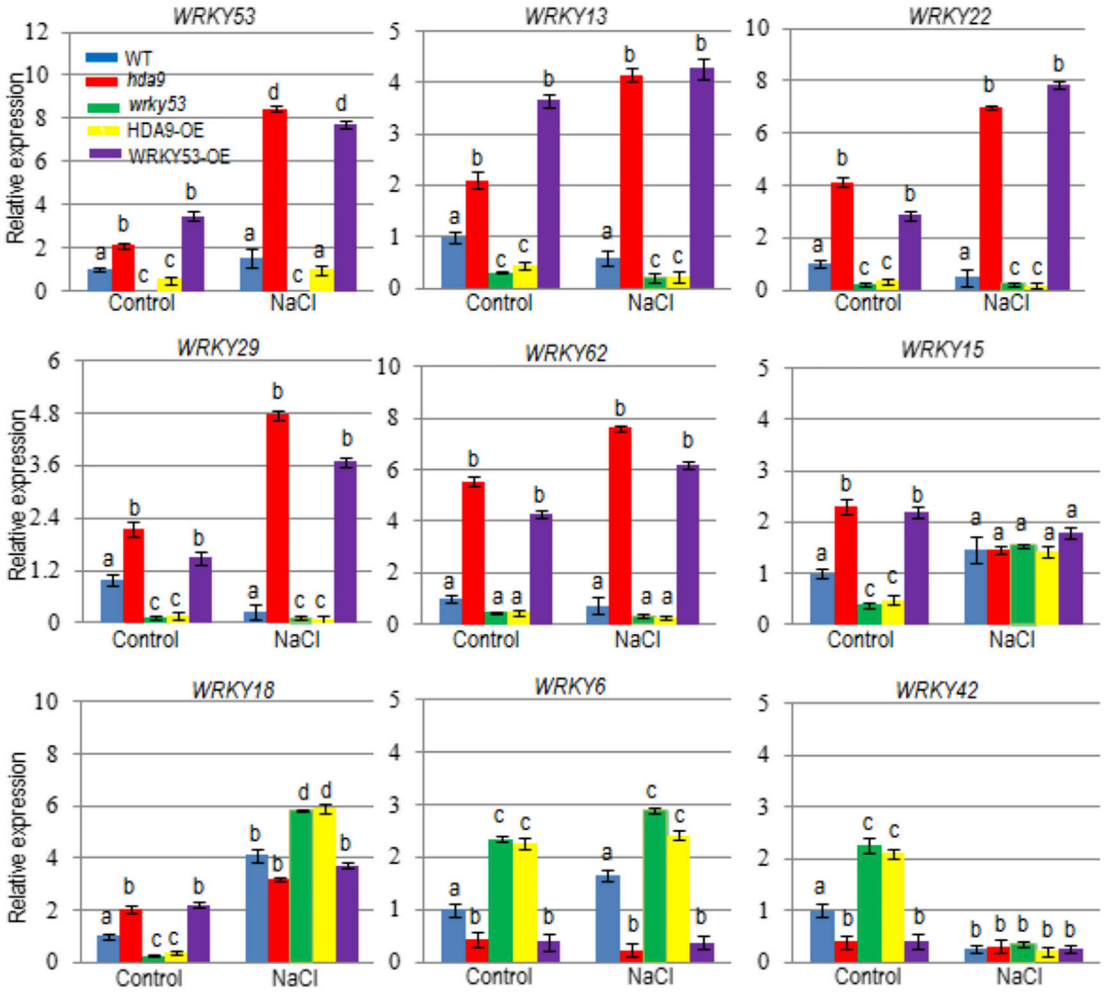

Figure 3. HDA9 Represses Expression of *WRKY53* and Its Downstream Targets.

Quantitative real-time PCR analysis of Expression of *WRKY53* and its downstream target WRKY genes in wild type (WT), *hda9-1*, *wrky53-1*, HDA9-OE (oe9-2), and WRKY53-OE (oe53-wt1) plants grown under normal (control) and 100 mM NaCl conditions for 30 days. Bars represent means ± SE from three biological replicates, and multiple comparison tests (Fisher's LSD) were conducted to analyze significant differences among samples. Different letters represent significant differences between samples.

in comparison with wild type. We found that, under normal conditions, the expression levels of *WRKY13*, *WRKY15*, *WRKY18*, *WRKY22*, *WRKY29*, and *WRKY62* were all higher ($p < 0.05$, >two-fold) in *hda9-1* and WRKY53-OE (oe53-wt1) and lower ($p < 0.05$, >two-fold) in *wrky53-1* and HDA9-OE (oe9-2) than in wild type, whereas those of *WRKY6* and *WRKY42* were clearly reduced ($p < 0.05$, >two-fold) in *hda9-1* and WRKY53-OE, but increased ($p < 0.05$, >two-fold) in *wrky53-1* and HDA9-OE compared with wild type (Figure 3). The data confirmed the positive or negative regulation of the genes by WRKY53 and indicated that HDA9 negatively regulates the activity of WRKY53 to control the downstream target genes under normal conditions. Under salt (100 mM NaCl) stress, *WRKY13*, *WRKY22*, *WRKY29*, and *WRKY62* displayed similar expression profiles compared with normal conditions in the different genotypes. The lack of further significant induction of the downstream genes by salt stress suggested that their expression, controlled by increased WRKY53 activity in *hda9* and WRKY53-OE plants, might be already saturating. However, the expression of *WRKY18* was more induced in the *wrky53* mutant and HDA9-OE than in the WRKY53-OE, *hda9* mutant, or wild-type backgrounds, suggesting that the induction of the gene by salt stress was independent of WRKY53 and HDA9. *WRKY6* expression was unchanged under stress compared with under normal conditions. The expression of *WRKY15* and *WRKY42* displayed no difference in the different genotypes under stress. Thus, four of the six downstream genes activated by WRKY53 under normal conditions are controlled by WRKY53 and HDA9 under salt stress.

To test whether *WRKY13*, *WRKY22*, *WRKY29*, and *WRKY62* are direct targets of WRKY53 or HDA9, we performed chromatin immunoprecipitation (ChIP) analysis of the *wrky53*-complementation lines grown under normal conditions using anti-GFP and anti-HDA9 antibodies. The precipitated chromatin fragments were analyzed by qPCR using a primer set corresponding to the W-box-containing region and another primer set corresponding to the coding region of the genes (Supplemental Figure 5). The analysis revealed that WRKY53 bound to the W-box-containing promoters. However, HDA9 was not found to be associated

with the promoters. The results suggested that HDA9 might regulate WRKY53 function off of its chromatin targets.

Repression of *WRKY53* Expression by HDA9 Is Independent of Histone Deacetylation

Next, we examined whether HDA9-mediated repression of *WRKY53* transcription was achieved through histone deacetylation of the locus. By ChIP assay, we compared the levels of histone modifications (H3K9ac, H3K27ac, H3K4me2, H3K4me3, H3K27me2, and H3K27me3) in the *WRKY53* promoter and coding regions in wild-type, *hda9-1*, and HDA9-OE (oe9-2) plants grown under normal or salt-stressed conditions. Surprisingly, the analysis revealed no significant change ($p > 0.05$, <two-fold) in H3K9ac, H3K27ac, or H3K27me3 at the *WRKY53* locus in the different genotypes under both normal and stressed conditions, but significantly higher H3K4me2/me3 levels ($p < 0.05$, >two-fold) were observed in the promoter region under salt stress in *hda9-1* (Supplemental Figure 6). H3K4me2 and H3K4me3 are two marks associated with actively transcribed genes in both plants and animals (Lachner et al., 2004; Li et al., 2008). The increases in these marks correlated well with the high induction of *WRKY53* by salt stress in *hda9* (Figure 3). The data suggested that HDA9-mediated repression of *WRKY53* was independent of histone deacetylation of the locus and supported the above observation that HDA9 was not associated with the WRKY gene promoters.

HDA9 Regulates Lysine Acetylation of WRKY53 Protein

In addition to histones, many proteins, including transcription factors, also show lysine acetylation that controls their function (Shen et al., 2015). To study whether HDA9 regulates the transcriptional function of WRKY53 through lysine deacetylation, we immunoprecipitated the WRKY53-GFP protein from transgenic plants in the wild-type, *hda9-1*, and HDA9-OE backgrounds using anti-GFP antibody and analyzed WRKY53-GFP lysine acetylation levels by immunoblotting using an anti-acetylated lysine antibody. Higher and lower levels of WRKY53-GFP lysine acetylation were observed in *hda9-1* and HDA9-OE, respectively, than in the wild-type background (Figure 4A). To confirm the results, we incubated WRKY53-GFP and GFP alone immunoprecipitated from tobacco leaves with *E. coli*-produced HDA9-GST or GST alone (Supplemental Figure 2), and analyzed lysine acetylation levels by immunoblotting using anti-acetylated lysine. Incubation with HDA9-GST but not GST reduced the lysine acetylation level of WRKY53-GFP (Figure 4B). Immunoprecipitated GFP did not show any lysine acetylation signal (Figure 4B). To further study the lysine acetylation sites regulated by HDA9, we analyzed the immunoprecipitated WRKY53-GFP proteins incubated with or without HDA9-GST by mass spectrometry. The analysis detected seven acetylated lysine residues (K12, K26, K27, K58, K169, K175, and K268) in the absence of HDA9-GST and two acetylated lysine residues (K169 and K175) in the presence of HDA9-GST (Figure 4C and Supplemental Figure 8; Supplemental Table 1). The results indicated that WRKY53 was post-translationally modified by lysine acetylation, and that acetylation at most of the sites could be removed by HDA9. The HDA9-targeted acetylation sites were located outside the DNA-binding domain of WRKY53. Comparison of WRKY protein sequences revealed that most of HDA9-targeted Lys residues were not conserved in other WRKY proteins (Supplemental Figure 7), suggesting that HDA9 specifically regulates WRKY53 lysine acetylation.

HDA9 Inhibits Binding of WRKY53 to Its Own Promoter

It was shown that WRKY53 could bind to its own promoter and activate its own expression (Miao et al., 2004). To test whether HDA9 regulates WRKY53 DNA-binding activity, we produced WRKY53-GST (Supplemental Figure 2) and used the protein for gel mobility assays with the WRKY53 promoter region containing the W box (−470 to −380) or a mutant version labeled with biotin as probe. Clear binding of the protein to the wild-type but not the mutant promoter region was observed (Figure 5A). Incubation with HDA9-GST, but not SRT1-GST (Liu et al., 2017), reduced the binding signal (Figure 5A). To study whether HDA9 affects binding of WRKY53 to its promoter, we performed ChIP analysis of *35S:WRKY53-GFP* plants in the wild-type, *hda9-1*, and HDA9-OE backgrounds using anti-GFP. The precipitated chromatin fragments were analyzed by qPCR using a primer set corresponding to the W-box-containing region and another primer set corresponding to a more upstream region (Figure 5B). The analysis revealed that WRKY53 bound *in vivo* to the W-box-containing promoter sequence. The amount of binding was significantly higher in the *hda9-1* mutant background, confirming that HDA9 inhibited WRKY53 binding to its target promoter. However, HDA9-OE had no clear effect on binding, suggesting that endogenous HDA9 might not be a limiting factor in the regulation of WRKY53 binding activity. In addition, there was no clear difference observed in plants grown on 1/2MS supplemented with 100 nM trichostatin A (TSA; an inhibitor of HDAC) or without TSA (Figure 5B), suggesting that the negative effect of HDA9 on WRKY53 DNA-binding activity was independent of lysine deacetylation. This was consistent with the observation that the lysine deacetylation sites targeted by HDA9 were located outside the DNA-binding domain of WRKY53 (Figure 4C).

HDA9 Inhibits the Transactivation Function of WRKY53

To study whether HDA9 regulates WRKY53 transcription activity, we co-transformed leaf protoplasts isolated from wild-type, *hda9-1*, and HDA9-OE (oe9-2) plants with *p*WRKY53Pro:GUS (reporter) and *p*35S:WRKY53-GFP (effector) or *p*35S:GFP as an effector control in the presence or absence of TSA. GUS activities were determined to analyze the effect of the *hda9-1* mutation and HDA9-OE on *WRKY53* autoactivation. In wild-type protoplasts, we detected significantly higher GUS activity in protoplasts transfected with *p*35S:WRKY53-GFP compared with those transfected with the *p*35S:GFP control (Figure 5C). Treatment with TSA further increased the GUS activity. In *hda9-1* protoplasts transformed with *p*35S:WRKY53-GFP, the GUS activity was much higher than that in wild type. However, TSA treatment did not reduce the activity. By contrast, in HDA9-OE protoplasts transformed with *p*35S:WRKY53-GFP, the GUS activity was at the same level as the control, suggesting that endogenous HDA9 might not be a limiting factor in the inhibition of WRKY53. Treatment with TSA increased the GUS activity. These results suggested that HDA9 represses the transcriptional activity of WRKY53, which is sensitive to TSA.

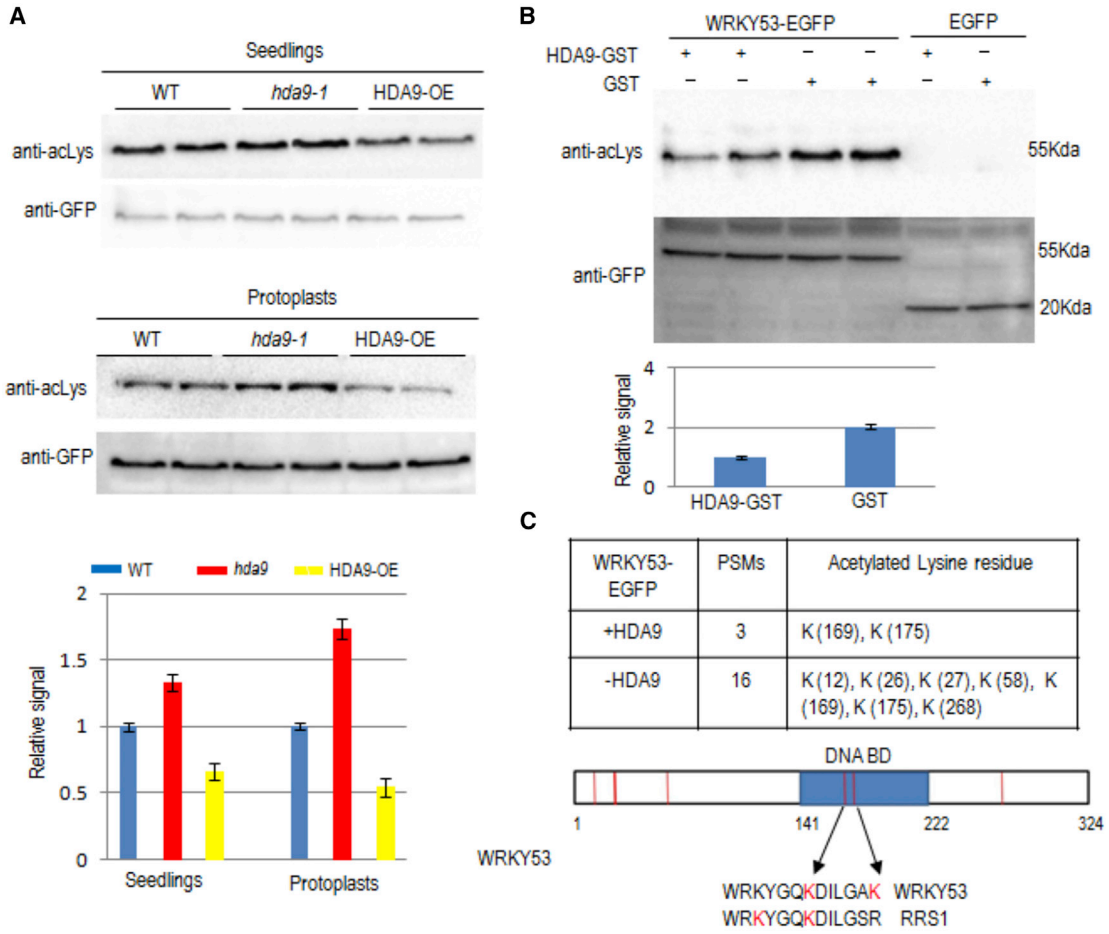

Figure 4. WRKY53 Displays Lysine Acetylation that Is Removed by HDA9.

(A) Lysine acetylation levels of WRKY53-GFP produced in wild-type, *hda9-1*, and HDA9-OE seedlings (top) or leaf protoplasts (middle). WRKY53-GFP was immunoprecipitated from the different genotypes and analyzed by immunoblotting with an antibody to acetylated lysine (anti-acLys). Anti-GFP was used as a loading control. The bands were quantified with ImageJ software. Bars are means ± SD from three measures of each of the two repeats.

(B) HDA9-GST could reduce the lysine acetylation level of WRKY53-GFP. WRKY53-GFP or GFP alone expressed in tobacco leaves was immunoprecipitated by anti-GFP and incubated with or without HDA9-GST or GST alone. The samples were then analyzed by immunoblotting with anti-acLys. Anti-GFP was used as a loading control. The bands were quantified with ImageJ software. Bars are means ± SD from three measures of each of the two repeats.

(C) Analysis of WRKY53 lysine acetylation sites by mass spectrometry. WRKY53-GFP was transiently expressed in tobacco leaves and purified with anti-GFP antibody-conjugated magnetic beads and incubated with *E. coli*-produced HDA9-GST or GST alone. Then the mixtures were resolved by SDS–PAGE and the WRKY53-GFP bands were excised for mass spectrometry analysis. The positions of detected lysine acetylation sites (red lines) are indicated. Sequence alignment shows comparison of the two lysine acetylation sites (in red) in the WRKY53 and RRS1 WRKY DNA-binding domains. The mass spectrometry graphs are shown in Supplemental Figure 8.

To further study the role of lysine acetylation in WRKY53 transcriptional function, we made Lys-to-Arg substitution mutations (to conserve the positive charge) of K169 and K175 and constructed the *p*35S:WRKY53M-GFP effector vector. The reporter (pWRKY53Pro:GUS) and the wild-type (*p*35S:WRKY53-GFP) or the mutant (*p*35S:WRKY53M-GFP) effector were co-transfected into *Arabidopsis* leaf protoplasts. GUS activities were significantly reduced in protoplasts transfected with p35S:WRKY53M-GFP compared with those transfected with *p*35S:WRKY53-GFP (Figure 5D). Treatment with TSA highly increased the GUS activity in protoplasts transfected with *p*35S:WRKY53-GFP and slightly increased it in those transfected with p35S:WRKY53M-GFP. The results indicated that lysine acetylation is important for the transactivation function of WRKY53.

WRKY53 Inhibits HDA9 Histone Deacetylase Activity

To study whether the mutation or overexpression of HDA9 affects histone acetylation, we compared histone acetylation levels of *HDA9* mutant and OE lines with those of wild-type plants by immunoblotting using anti-H3K9ac, anti-H3K27ac, anti-H3ac, and anti-H3 antibodies. The analysis revealed clear increases of H3K9ac and H3K27ac levels in *hda9* and slight decreases of the levels in HDA9-OE compared with wild-type plants, while no clear change in overall H3 acetylation level was observed

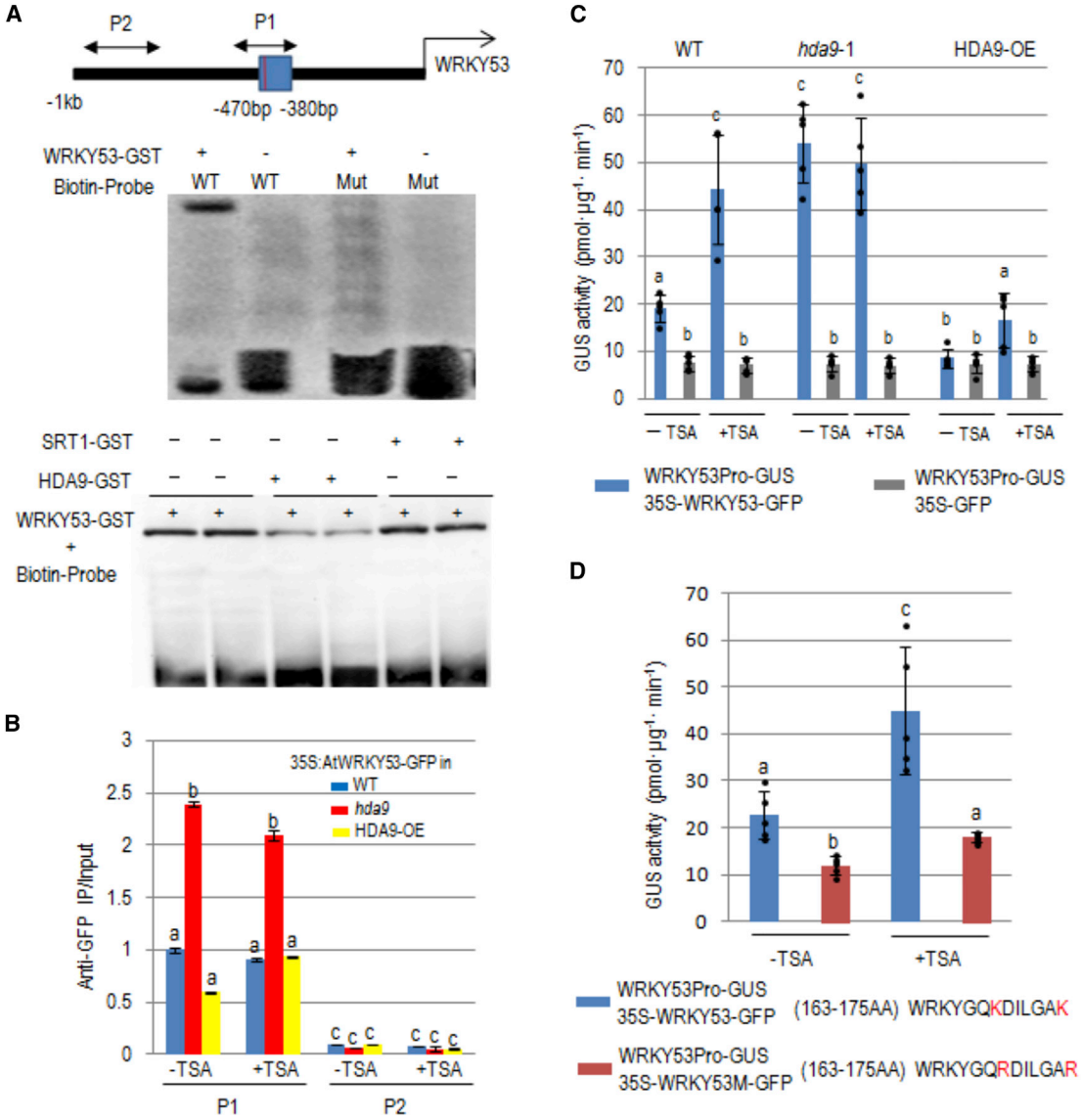

Figure 5. HDA9 Inhibits the DNA-Binding and Transcriptional Activity of WRKY53.

(A) DNA binding of WRKY53 is impaired by HDA9 *in vitro*. Electrophoretic mobility shift assay (EMSA) of WRKY53-GST binding to its promoter region is shown. (Top) Blue box represents the probe and the red line indicates the W-box motif (TTGACC), which was substituted with (TTGAAA) in the mutated probe. Both wild-type and mutant versions of the promoter fragment were biotin labeled and used for incubation with or without WRKY53-GST (middle). (Bottom) EMSA of WRKY53-GST binding to the wild-type promoter region in the presence or absence of HDA9-GST or SRT1-GST.

(B) ChIP-PCR analysis of WRKY53-GFP association with its promoter regions in *wrky53-1*, *hda9-1*, and HDA9-OE plants treated with or without TSA. Two regions (P1 and P2) of the locus, shown in (A), were tested. Bars represent means ± SE from three biological replicates, and multiple comparison tests (Fisher's LSD) were conducted to analyze significant differences among samples. Different letters represent significant differences between samples.

(C) Transient expression assays of the *p*WRKY53Pro:GUS reporter in protoplasts isolated from wild-type (WT), *hda9-1*, and HDA9-OE (oe9-2) plants with or without TSA treatment. The protoplasts were co-transformed with the reporter (*p*WRKY53Pro:GUS) and the effector (*p*35S:WRKY53-GFP) or the control (35S:GFP) vector, and GUS enzyme activity was measured after 30 min. Bars represent means ± SE from three biological replicates, and multiple comparison tests (Fisher's LSD) were conducted to analyze significant differences among samples. Different letters represent significant differences between samples.

(D) Transient expression assays of protoplasts co-transformed with the reporter (*p*WRKY53Pro:GUS) and the wild-type effector (*p*35S:WRKY53-GFP) or the mutant effector (*p*35S:WRKY53M-GFP) vector. Protoplasts were isolated from *Arabidopsis* plants treated with or without TSA. GUS enzyme activity was measured after 30 min. Bars represent means ± SE from three biological replicates, and multiple comparison tests (Fisher's LSD) were conducted to analyze significant differences among samples. Different letters represent significant differences between samples.

(Figure 6A). This was consistent with previous results showing that HDA9 is involved in deacetylation of H3K9ac and H3K27ac (Kim et al., 2016). Interestingly, we found increased levels of H3K9ac and H3K27ac in WRKY53-OE and decreased levels in *wrky53-1* plants. This observation raised the possibility that WRKY53 might also regulate the activity of HDA9.

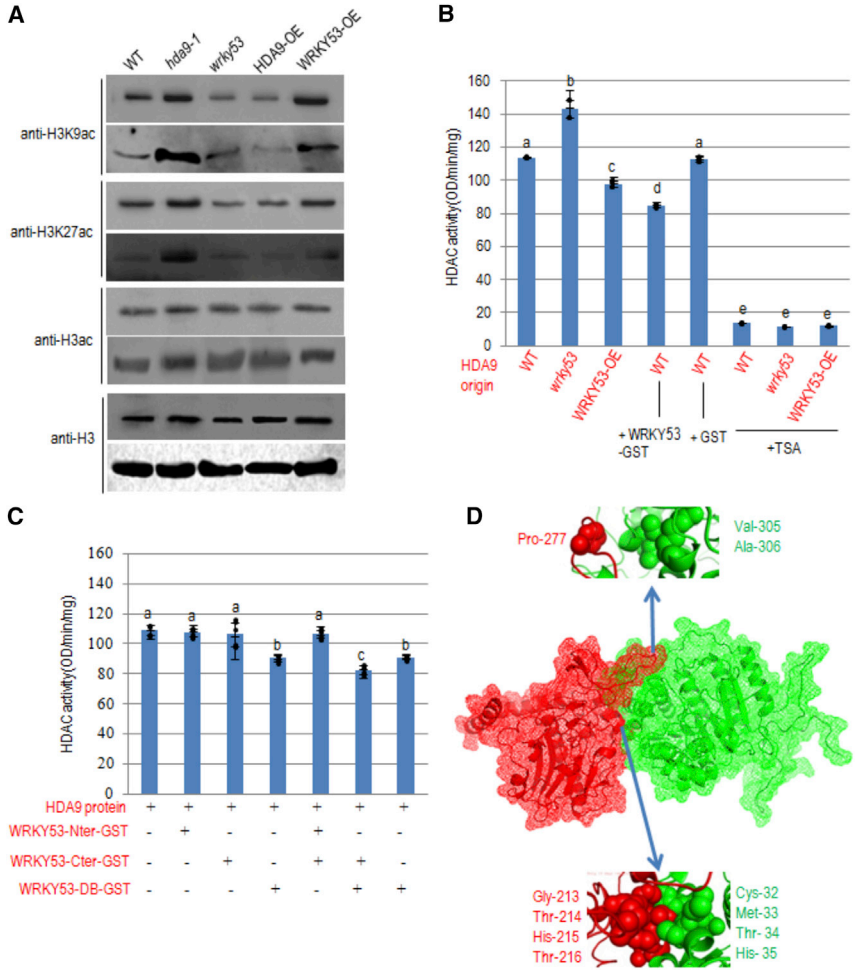

Figure 6. WRKY53 Shows an Inhibitory Effect on HDA9 Deacetylase Activity.

(A) WRKY53 affects histone acetylation in plants. Histone acetylation levels were detected by immunoblotting with antibodies against the indicated histone acetylation marks in wild-type (WT), *hda9*, *wrky53*, HDA9-OE (oe9-2), and WRKY53-OE (oe53-wt1) seedlings. Two repeats of the immunoblots are shown. Anti-H3 antibody was used to control for loading.

(B) *In vitro* deacetylase activity assays. HDA9 protein was isolated by immunoprecipitation with anti-HDA9 from wild-type, *wrky53-1*, and WRKY53-OE plants, and the HDAC activity was assayed in the presence of *E. coli*-produced WRKY53-GST or GST alone. TSA was added to the assays as a control. The deacetylase activity is expressed as relative fluorescence intensity determined using a fluorescence microplate reader. Bars represent means ± SE from three biological replicates, and multiple comparison tests (Fisher's LSD) were conducted to analyze significant differences among samples. Different letters represent significant differences between samples.

(C) *In vitro* HDA9 HDAC activity assays. HDA9 protein was isolated by immunoprecipitation with anti-HDA9 from wild-type plants. HDAC activity was assayed in the presence of WRKY53-Nter-GST, WRKY53-Cter-GST, or WRKY53-DB-GST. The deacetylase activity is expressed as relative fluorescence intensity determined using a fluorescence microplate reader. Bars represent means ± SE from three biological replicates, and multiple comparison tests (Fisher's LSD) were conducted to analyze significant differences among samples. Different letters represent significant differences between samples.

(D) Computational model of protein interaction between HDA9 (green) and WRKY53 (red). Residues Gly213, Thr214, His215, and Thr216 within the WRKY53 DNA-binding domain make direct contacts with Cys32, Met33, Thr34, and His35 within the HDA9 HDAC domain. Pro277 of WRKY53 is close to Val305 and Ala306 of HDA9.

To test this hypothesis, we immunopurified HDA9 protein from wild-type (Col-0), *wrky53* mutant (*wrky53-1*), and OE-WRKY53 (oe53-wt-1) plants grown under normal conditions using anti-HDA9 antibody and measured HDAC activity using the Epigenase HDAC activity/inhibition direct assay kit. The tests revealed higher HDAC activity of HDA9 isolated from *wrky53* and lower activity of the protein isolated from WRKY53-OE compared with that isolated from wild-type plants (Figure 6B). The HDAC activities were largely reduced in the presence of TSA. We also tested the HDAC activity of the HDA9 protein isolated from wild-type plants by adding *E. coli*-produced WRKY53-GST or GST alone in the assays. The tests indicated that WRKY53-GST, but not GST alone, reduced the *in vitro* HDAC activity of HDA9. To test whether WRKY53 interaction affects HDA9 HDAC activity, we separated WRKY53 into N-terminal (Nter), DNA-binding (DB), and C-terminal (Cter) regions (Figure 1D) and produced WRKY53-Nter-GST, WRKY53-DB-GST, and WRKY53-Cter-GST proteins in *E. coli* (Supplemental Figure 2). The proteins were included in HDA9 HDAC activity assays. The presence of WRKY53-Nter-GST, WRKY53-Cter-GST, or both had no effect on the HDAC activity of HDA9 isolated from wild-type plants. By contrast, WRKY53-DB-GST significantly reduced HDA9 activity (Figure 6C), suggesting that the interaction between the WRKY53 DB domain and HDA9 inhibited the HDAC activity. Computational analysis of a putative interaction docking model revealed that four residues (Gly213, Thr214, His215, and Thr216) located in the DB domain of WRKY53 were in contact with four residues (Cys32, Met33, Thr34, and His25) in the catalytic domain of HDA9. In addition, Pro277 of WRKY53 was found to be close to Val305 and Ala306 of HDA9 (Figure 6D). The contacting residues in WRKY53 and HDA9 are not conserved in other WRKY or HDAC proteins, supporting the above finding that the interaction between the two proteins was specific. The interaction might mask HDA9 HDAC activity.

DISCUSSION

HDA9 and WRKY53 Antagonistically Regulate Plant Response to Stress

Recent results have shown that HDA9 acts in a complex with a SANT domain-containing protein, POWERDRESS, and WRKY53 to promote age-related and dark-induced leaf senescence (Chen et al., 2016; Kim et al., 2016). However, the precise molecular

function of WRKY53 in the complex is not yet known. The present work showing mutual inhibition between HDA9 and WRKY53 in regulating stress response suggests that the two proteins may antagonistically regulate gene expression in multiple pathways.

We have previously reported that HDA9 has a negative function in salt stress responses. HDA9 represses a large number of stress-responsive genes by regulating histone acetylation in their promoters (Zheng et al., 2016). In this study, we provide evidence that HDA9 interacts with and inhibits the DNA binding and transcriptional activity of WRKY53 to repress *WRKY53* autoactivation and activation of its downstream WRKY genes (which are also stress regulators) under both normal and stressed conditions, indicating that HDA9 constitutively inhibits the gene regulatory network controlled by WRKY53. The higher stress tolerance of *hda9* mutants and impaired stress tolerance of HDA9-OE plants (Figure 2) are at least in part related to the derepressed and inhibited transcription activity of WRKY53, respectively. Thus, the negative function of HDA9 in stress tolerance may be achieved by repressing the DNA-binding and transcriptional activity of WRKY53 in addition to mediating histone deacetylation of other stress-responsive genes. Similar, previous results showed that HDA19 interacts with WRKY38 and WRKY62 and has an antagonistic function toward the transcription factors in basal defense (Kim et al., 2008).

HDA9-Mediated Lysine Deacetylation Inhibits WRKY53 Transcriptional Activity

Previous work showed that the WRKY DNA-binding domain of the RRS1 protein can be lysine acetylated by the bacterial pathogen effector PopP2, resulting in inhibition of DNA-binding activity (Sarris et al., 2015). The present work revealed several lysine acetylation sites in WRKY53, including two sites within the WRKY DNA-binding domain, and that HDA9 could remove acetylation from most of the sites except those within the DNA-binding domain (Figure 4), which actually interacted with the catalytic domain of HDA9 (Figure 1). In the RRS1 WRKY domain, two lysine residues are acetylated (Sarris et al., 2015). One of these acetylation sites was also identified in the WRKY53 DNA-binding domain (Figure 4C). The observation that TSA treatment did not affect HDA9 inhibition of WRKY53 binding to its target sequence *in vivo* (Figure 5B) suggests that HDA9 inhibition of WRKY53 DNA-binding activity may be independent of lysine deacetylation and simply due to physical interaction. By contrast, HDA9-mediated lysine deacetylation was involved in the inhibition of WRKY53 transcription activity, as the inhibitory effect of HDA9 could be alleviated by addition of TSA in the transient expression assays in HDA9-OE or wild-type protoplasts (Figure 5C). The results showing that Lys-to-Arg substitution mutation of WRKY53 reduced the transactivation function (Figure 5D) confirm that WRKY53 transcriptional activity is modulated by lysine acetylation. The effects of HDA9 on WRKY53 lysine acetylation indicate that, in addition to histones, HDA9 also deacetylates non-histone proteins to regulate gene expression. Evidence for the regulation of transcription factor activity by HDAC-mediated lysine deacetylation is emerging in plants (Hartl et al., 2017). For instance, HDA6 can interact with and deacetylate BIN2 to repress its kinase activity in *Arabidopsis* (Hao et al., 2016). The *Arabidopsis* sirtuin-like HDAC SRT1 deacetylates and enhances the stability of AtMBP-1, a transcriptional repressor of stress-responsive and glycolytic genes (Liu et al., 2017). Similarly, rice SRT1 could deacetylate glyceraldehyde-3-phosphate dehydrogenase and inhibit its nuclear localization and function as a transcriptional activator of glycolytic genes (Zhang et al., 2017).

WRKY53 has been reported to play a central role in several stress pathways, including senescence regulation (Hinderhofer and Zentgraf, 2001; Miao and Zentgraf, 2007; Zentgraf et al., 2010), drought stress response (Sun and Yu, 2015), and basal resistance against *Pseudomonas syringae* (Murray et al., 2007). The present data confirmed that WRKY53 functions as a high-hierarchical transcriptional regulator of downstream stress-responsive WRKY genes. In addition, our data suggest that WRKY53 may also enhance stress tolerance by inhibiting HDA9 HDAC activity. Although the precise mechanism of the inhibition remains unclear at this stage, our data suggest that interaction with WRKY53 may mask the HDAC activity of HDA9 or prevent its targeting to genomic loci for histone deacetylation. Thus, HDA9 and WRKY53 form an antagonistic pair reciprocally repressing each other's activities.

In conclusion, our results indicate that HDA9 represses stress-responsive gene expression by mediating lysine deacetylation of both histones and WRKY53, which, in its acetylated form, functions as a high-hierarchy activator of downstream WRKY genes. Conversely, WRKY53 can inhibit HDA9 HDAC activity (Figure 7). This work uncovers a functional interplay between a chromatin regulator (i.e., HDA9) and a transcription factor (i.e., WRKY53) that regulates stress resistance/tolerance.

METHODS

Plant Materials and Production of Transgenic Plants

The *Arabidopsis* ecotype Columbia-0 (Col-0) was used as wild type in all experiments. The *hda9* T-DNA mutants (*hda9-1*, SALK, N507123; *hda9-2*, GABI-kat, 305G0320) were previously reported (Kim et al., 2013). The T-DNA insertion mutants *wrky53-1* (SALK_034157) and *wrky53-2* (SALKSEQ_110288.2) were obtained from the *Arabidopsis* Biological Resource Center. After being surface sterilized in 30% bleach, *Arabidopsis* seeds were kept at 4°C for 48 h before sowing. All seeds, except those used in germination tests, were grown *in vitro* on half-strength MS medium with 0.5% sucrose (pH 5.7, 1.2% agar) in a growth chamber (20°C) under white light (120 μmol m^{-2} s^{-1}) under a 16 h light/day photoperiod for 10 days and then transplanted into soil. The same temperature, light intensity, and photoperiod were used for seedlings grown in soil.

For producing WRKY53 and HDA9-OE plants, the full-length cDNAs of *WRKY53* and *HDA9* were amplified and cloned into a modified *p*1300 vector (*p*35S:GFP) separately to obtain the *p*35S:HDA9-GFP and *p*35S:WRKY53-GFP vectors. These vectors were transformed by *Agrobacterium*-mediated infection into wild-type plants to obtain the HDA9-OE and WRKY53-OE lines. The *p*35S:WRKY53-GFP vector was also used to transform the *hda9-1* mutant and the *wrky53-1* mutant to obtain the WRKY53-OE-*hda9* and WRKY53-complementation lines. Two lines from each transgene were chosen for phenotype observation and analysis. Plants co-overexpressing HDA9 and WRKY53 were obtained by transforming the *p*35S:WRKY53-GFP vector into HDA9-OE (oe9-2).

Measurements of Salt Stress Response, Germination Rate, ABA Content, and Fresh Water Loss Rate of Detached Leaves

Salt stress was imitated by adding PEG (−0.75 MPa), NaCl (100 mM), and mannitol (150 mM) to MS medium (Verslues et al., 2006). For measuring germination, approximately 100 seeds were sown. The germination (fully

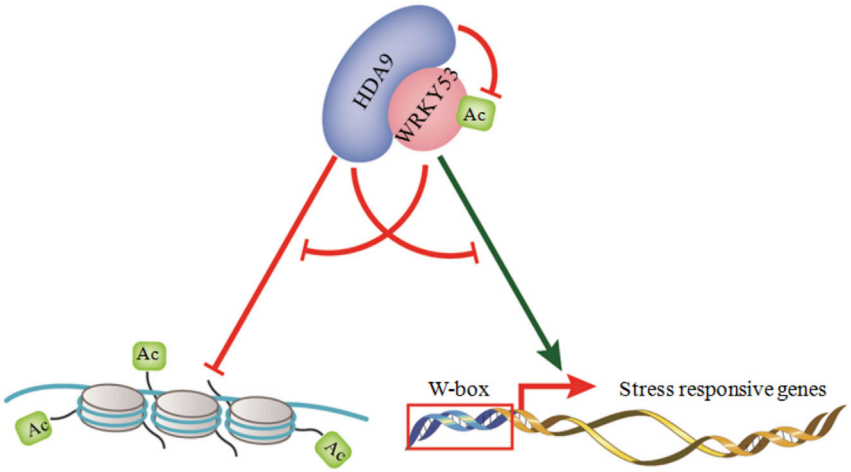

Figure 7. Proposed Model Deciphering the Functional Interaction between HDA9 and WRKY53 in the Regulation of Plant Stress Response.

HDA9 interacts with and reduces lysine acetylation of WRKY53, thereby inhibiting the transcriptional activity of WRKY53, which functions as a high-hierarchy activator of downstream W-box-containing stress-responsive WRKY genes. Conversely, WRKY53 reduces HDA9-mediated deacetylation of nucleosomal histones. Ac, lysine acetylation.

emerged radical) rates were scored after 78 h. Three seed batches (harvested in December 2016, March 2017, and May 2017) were used in germination tests to avoid harvest and storage effects. Two alleles of each mutant and two lines of each transgenic plant were tested with three biological repeats. For wild-type samples, six biological repeats were tested. Multiple comparisons using the LSD (Fisher's least significant difference) method were conducted to analyze significant differences among samples.

Seedlings grown in soil were treated with 100 mM NaCl (by pouring 100 mM NaCl into trays containing the seedling pots) for 30 days. Seedlings treated with water for the same period were used as controls. Photographs of plants were taken from different biological repetitions. ABA contents of two whole seedlings were determined by ELISA (Kmaels Biotechnology, Shanghai) by following the manufacturer's instructions. Three biological repetitions were performed. Water loss rates of detached leaves were assayed as described by Zhang et al. (2004) with minor modifications. The sixth rosette leaf from six plants per genotype was excised at the same developmental stage and exposed to light (110 μmol m^{-2} s^{-1}) at 22°C. The leaves for each repeat were weighed at various time points, and the loss of fresh weight (%) was used to represent water loss rate. Two alleles of each mutant and two lines of each transgene were tested with three biological repeats. For wild-type samples, six biological repeats were tested. Multiple comparisons using Fisher's LSD method were conducted to analyze significant differences among samples.

Yeast Two-Hybrid Assays

Full-length or fragmented cDNAs of *WRKY53*, *WRKY22*, *WRKY38*, *WRKY62*, *HDA9*, *HDA6*, *HDA19*, and *SRT1* were amplified by PCR and cloned into the prey vector *p*GADT7 or bait vector *p*GBKT7 (Clontech, USA). The DNA-binding motif of WRKY53 (421–663 bp) and the deacetylase motif of HDA9 (64–945 bp) were cloned into *p*GADT7 and *p*GBKT7, respectively. The N- (1–63 bp of HDA9, 1–420 bp of WRKY53) and C- (946–1278 bp of HDA9, 664–972 bp of WRKY53) terminal fragments were also ligated into both the prey and the bait vectors.

Y2H assays were performed using the Matchmaker Gold two-hybrid system following the manufacturer's protocols. In this study, SD/−Leu/−Trp dropout medium (double-dropout medium) was used to select for the bait and prey plasmids. Cells harboring Matchmaker bait and prey plasmids were able to grow because the plasmids encode tryptophan and leucine biosynthesis genes, respectively, which were otherwise absent from the cell. SD/−Ade/−His/−Leu/−Trp dropout medium (quadruple-dropout medium) was used to confirm protein interactions through activation of *HIS3* and *ADE2*.

Co-immunoprecipitation Analysis

The anti-HDA9 antibody was produced using peptides synthesized by ABclonal Biotech, Wuhan, China. Co-IP was performed using *WRKY53* overexpression plants (oe53-wt-1). Total proteins extracted from 1.5 g plant materials were incubated with 50 ml protein A magnetic beads (Thermo Fisher Scientific 88802) and anti-GFP (Abcam ab13970) for WRKY53-GFP purification or anti-HDA9 for HDA9 purification. Total and immunoprecipitated proteins were detected by immunoblotting with anti-GFP and anti-HDA9 antibodies using the ECL SuperSignal system.

Bimolecular Fluorescence Complementation Experiments

For BiFC, HDA9 and WRKY53 were tagged with the N-terminal part (YFPN) and the C-terminal part (YFPC) of YFP, respectively, as previously described (Schütze et al., 2009). The two vectors were co-transformed into *Arabidopsis* mesophyll protoplasts as previously described (Yoo et al., 2007). DAPI staining was used to visualize the nuclei. The fluorescence was observed with a laser scanning confocal microscope (Leica DM IRE2). The empty vectors pYFPC and *p*WRKY53-YFPN were co-transformed into *Arabidopsis* protoplasts as the negative control.

Quantitative Real-Time PCR Analysis of Gene Expression

Total RNA was extracted from seedlings grown in soil with or without NaCl treatment using Trizol isolation reagents, and first-strand cDNA was synthesized from 1 μg of total RNA using the First Strand cDNA Synthesis Kit (Transgene Biotech) following the manufacturer's protocol. Three biological replicates for each sample were used for RNA extraction. For quantitative real-time PCR assays, transcript levels were normalized against the average of the reference genes: *tubulin2* (AT5G62690) and *actin2* (AT3G18780). The Ct values and the real-time PCR efficiencies were obtained using LinRegPCR (12.X) (Ruijter et al., 2009), and then the normalized relative quantities and standard errors for each sample were obtained by pBaseplus (Hellemans et al., 2007). The relative fold differences in gene expression in different samples were calculated on the basis of the normalized relative quantities obtained above, with the normalized relative quantity of wild type (control) set as 1. Each biological replicate had three technical repetitions, and reaction mixtures without cDNA templates were used as negative controls to evaluate the specificity of each real-time PCR. Multiple comparisons using Fisher's LSD method were conducted to analyze significant differences among samples. The primers for all genes and annealing temperatures used in quantitative real-time PCR are given in Supplemental Table 2.

Chromatin Immunoprecipitation Assay

Chromatin fragments were isolated from seedlings of wild-type and mutant or transgenic plants and immunoprecipitated with antibodies to H3K9ac (Millipore, 07-352), H3K27ac (Millipore 05-1334), H3K27me2 (Millipore 07-452), H3K27me3 (Millipore 07-449), H3K4me2 (Millipore 07-030), and

H3K4me3 (Millipore 07-473). The amounts of immunoprecipitated chromatin fragments relative to input chromatin were determined by qPCR analysis using two primer pairs specific to *WRKY53* and calculated according to the $2^{-\Delta\Delta CT}$ method.

To analyze WRYK53-GFP binding to the *WRKY53* promoter *in vivo*, we used anti-GFP to immunoprecipitate the chromatin fragments isolated from transgenic plants expressing WRKY53-GFP and analyzed relative enrichment (immunoprecipitation/input) of two *WRKY53* promoter regions of by qPCR.

To analyze whether *WRKY13*, *WRKY22*, *WRKY29*, and *WRKY62* are direct targets of WRKY53 or HDA9, we performed ChIP–PCR analysis of WRKY53-complementation lines grown under normal conditions using anti-GFP and anti-HDA9.

Each sample had three biological replicates, and multiple comparisons using Fisher's LSD method were conducted to analyze significant differences among samples. The primer pairs used for ChIP–PCR are listed in Supplemental Table 2.

Immunoblotting Analysis of WRKY53 and Histone Lysine Acetylation

To detect lysine acetylation of the WRKY53 protein, 5 week old wild-type (oe53-wt-1), *hda9* mutant (oe53-hda9-1), and OE-HDA9 (oe53-oe9-2) seedlings overexpressing WRKY53-GFP were used to isolate total proteins. The same plant materials were also used to prepare mesophyll protoplasts for total protein extraction. In addition, *p*35S:WRKY53-GFP and *p*35S:GFP were introduced into 5 week old tobacco (*Nicotiana benthamiana*) leaf cells by injection (5 weeks) and total proteins were extracted. WRKY53-GFP or GFP proteins from the above protein extracts were purified using anti-GFP agarose after a series of washing steps. Eluted proteins were detected by immunoblotting with anti-GFP (Abcam ab13970) and anti-acetyl lysine (Abcam ab80178) antibodies using the ECL Super-Signal system.

For histone acetylation analysis, histone proteins were extracted from 1.5 g of plant tissues of wild-type and F2 transgenic lines as previously described (Benhamed et al., 2006). Antibodies to H3K9ac (Millipore, 07-352), H3K27ac (Millipore 05-1334), H3ac (Active Motif, 39139), and H3 (Abcam, ab1791) were used. All immunoblots were developed using the ECL SuperSignal system.

Transient Expression Assays

For transient expression assays in *Arabidopsis* protoplasts, the 1 kb promoter of *WRKY53* was amplified and cloned upstream of the *GUS* coding sequence in a modified *p*1301 binary vector to obtain the *p*WRKY53Pro:GUS reporter vector. *p*35S:WRKY53-GFP was used as the effector vector and *p*35S:GFP as the effector control vector. Lysines 169 and 175 of WRKY3 cDNA were mutated to arginine using the One Tube Fast Mutagenesis Kit (Aidlab Biotechnologies) and the mutated *WRKY53* cDNA was cloned into the *p*35S:GFP vector to obtain the effector vector *p*35S:WRKY53M-GFP. Seedlings (5 weeks old) of wild-type (Col-0), *hda9* mutant *(hda9-1)*, *wrky53* mutant (*wrky53-1*), and HDA9 overexpression lines (oe9-2) grown on 1/2MS or 1/2MS supplemented with TSA (100 nM) were used to produce *Arabidopsis* mesophyll protoplasts. Co-transformation of *Arabidopsis* mesophyll protoplasts was performed as previously described (Yoo et al., 2007). GUS activity assays were carried out as described by Schledzewski and Mendel (1994).

Electrophoretic Mobility Shift Assays

The full-length coding sequences of *HDA9* and *WRKY53* were cloned into a modified *p*TOPO-D1 vector and transformed into *E. coli* strain BL21 (DE3). The recombinant proteins were affinity purified using the GST label protein purification kit (Beyotime Biotechnology).

For the electrophoretic mobility shift assay (EMSA), the WRKY53 promoter region containing the WRKY box (−470 to −380) was used as probe. The same region without the WRKY box was used as mutated probe by substituting the 5′-TTGACC-3′ motif with 5′-TTGAAA-3′ (Supplemental Table 2). All the probes were synthesized and biotin labeled by Beyotime Biotechnology. EMSAs were performed using the LightShift Chemiluminescent EMSA Kit (Thermo Scientific, Waltham, MA, USA) according to the manufacturer's instructions. The WRKY53-GST and HDA9-GST fusion proteins were mixed with biotin-labeled wild-type or mutant probes and incubated at 24°C for 30 min. The unlabeled probes were used for competition assays. The free and bound probes were separated by acrylamide gel electrophoresis.

Liquid Chromatography–Tandem Mass Spectrometry and Data Processing

Total proteins were extracted from tobacco leaves expressing WRKY53-GFP and immunoprecipitated with anti-GFP antibody-conjugated magnetic beads. Next, 0.5 g of the eluate was incubated with *E. coli*-produced HDA9-GST or GST protein in HDAC assay buffer (1.4 mM NaH_2PO_4, 18.6 mM Na_2HPO_4, 0.25 mM EDTA, 10 mM NaCl, 10% [v/v] glycerol, and 10 mM β-mercaptoethanol). The deacetylation assay was performed as described (Zhang et al., 2017; Lu et al., 2018). Then the two mixtures were resolved by SDS–PAGE. The WRKY53-GFP bands were excised from the SDS–PAGE gel, fully trypsinized, and analyzed on a Thermo Fisher LTQ Obitrap ETD mass spectrometer. Briefly, samples were loaded onto a high-pressure liquid chromatography system, named Thermo Fisher Easy-nLC 1000, equipped with a C18 column (1.8 mm, 0.15 × 100 mm). Solvent A contained 0.1% formic acid and solvent B contained 100% acetonitrile. The elution gradient was from 4% to 18% solvent B in 182 min, 18% to 90% solvent B in 13 min at a flow rate of 300 nL/min. Mass spectrometry analysis was carried out at AIMS Scientific (Shanghai, China) in the positive-ion mode, with an automated data-dependent tandem mass spectrometry (MS/MS) analysis with full scans (350–1600 m/z) acquired using Fourier transform mass spectrometry at a mass resolution of 30 000, and the 10 most intense precursor ions were selected for MS/MS. The MS/MS spectra were acquired using higher-energy collision dissociation at 35% collision energy at a mass resolution of 15 000. Raw mass spectrometry files were analyzed by Proteome Discoverer 1.4 with TAIR data (uniprot-Arabidopsis thaliana.fasta). The related parameters used for the raw mass spectrometry files analyzed were as follows: EnFLAGme Name was Trypsin (full); Max.Missed Cleavage Sites were 2; Static Modification was Carbamidomethyl (C); Dynamic Modification was Oxidation (M), Deamidated (N,Q), Acetyl(K); Precursor Mass Tolerance was 20 ppm; Fragment Mass Tolerance was 0.05D; Validation based on q-Value. The mass spectrometry files were uploaded to the iProX databases under accession no. PXD016822.

In Vitro HDAC Assays of HDA9 Protein Isolated from Plant Extracts

HDA9 protein was immunopurified using anti-HDA9 and protein A beads from total protein extracts of wild-type (Col-0), *wrky53* mutant (*wrky53-1*), and WRKY53 OE (oe53-wt-1) plants grown under normal conditions. After incubation at 4°C overnight, HDA9 was eluted from the protein A beads after a series of washes. HDA9 protein (about 0.2 μg) was used to test *in vitro* HDAC activity. An Epigenase HDAC Activity/Inhibition Direct Assay Kit (Epigentek) was used to measure the HDAC activity according to the manufacturer's instructions. The fluorescence was read on a fluorescence microplate reader within 2–10 min at 530EX/590EM. The HDAC inhibitor TSA (100 nM) was used. The activity of the

HDAC enzyme in proportion to the OD intensity was calculated with formula:

$$\text{HDAC Activity (RFU / min / mg)} = \frac{\text{Sample RFU} - \text{Blank RFU}}{\text{Protein Amount } (\mu g) * \times \text{min} * *} \times 1000$$

Protein Structural Modeling

A homology model of the three-dimensional structure of WRKY53 and HDA9 predicted based on their sequence similarity to five proteins of known structure was downloaded from the PDB database (http://www.rcsb.org/). Protein structure files 1wj2.pdb, 22yd.pdb, 2lex.pdb, 5w3x.pdb, and 6ir8.pdb were used as templates for WRKY53, and protein structure files 4bkx.pdb, 5icn.pdb, 4a69.pdb, 4lxz.pdb, and 4ly1 were used as templates for HDA9. Homology modeling was performed with MODELLER (https://salilab.org/modeller/). The model with the lowest energy and highest score was selected for further docking analysis. ZDOCK (http://zdock.umassmed.edu/) was used for primary docking, and the top 1 model produced by ZDOCK was optimized by PyROSETTA (http://www.pyrosetta.org/) according to the software's protein–protein interaction protocol. Structural figures were prepared using PyMOL (https://pymol.org/2/).

SUPPLEMENTAL INFORMATION

Supplemental Information is available at *Molecular Plant Online*.

FUNDING

This study was supported by the Discipline Innovation Team Foundation of Jianghan University (03100074), Natural Science Foundation of Hubei Province (grant no.2016CFB630), National Natural Science Foundation of China (NSFC31701100, NSFC31600981, and NSFC31600801), and French ANR-19-CE12-0027-01.

AUTHOR CONTRIBUTIONS

Conceptualization, Y.Z. and D.X.Z.; Investigation, Y.Z., J.Y.G., C.B., J.J.L., J.J.S., X.Y.L., L.F.S., and L.P.; Formal Analysis, Y.Z. and C.B.; Visualization, Y.Z.; Writing – Original Draft, Y.Z. and D.X.Z.; Writing – Review & Editing, Y.Z. and D.X.Z.; Funding Acquisition, Y.Z., X.Y.L., L.P., and D.X.Z.

ACKNOWLEDGMENTS

No conflict of interest declared.

Received: July 12, 2019
Revised: December 23, 2019
Accepted: December 23, 2019
Published: December 27, 2019

REFERENCES

Alinsug, M.V., Yu, C.-W., and Wu, K. (2009). Phylogenetic analysis, subcellular localization, and expression patterns of RPD3/HDA1 family histone deacetylases in plants. BMC Plant Biol. **9**:37.

Benhamed, M., Bertrand, C., Servet, C., and Zhou, D.-X. (2006). *Arabidopsis* GCN5, HD1, and TAF1/HAF2 interact to regulate histone acetylation required for light-responsive gene expression. Plant Cell **18**:2893–2903.

Bohnert, H.J., Gong, Q., Li, P., and Ma, S. (2006). Unraveling abiotic stress tolerance mechanisms–getting genomics going. Curr. Opin. Plant Biol. **9**:180–188.

Chen, L.-T., and Wu, K. (2010). Role of histone deacetylases HDA6 and HDA19 in ABA and abiotic stress response. Plant Signal. Behav. **5**:1318–1320.

Chen, L.-T., Luo, M., Wang, Y.-Y., and Wu, K. (2010). Involvement of *Arabidopsis* histone deacetylase HDA6 in ABA and salt stress response. J. Exp. Bot. **61**:3345–3353.

Chen, X., Lu, L., Mayer, K.S., Scalf, M., Qian, S., Lomax, A., Smith, L.M., and Zhong, X. (2016). POWERDRESS interacts with HISTONE DEACETYLASE 9 to promote aging in Arabidopsis. Elife **5**:e17214.

Chen, Q., Xu, X., Xu, D., Zhang, H., Zhang, C., and Li, G. (2019). WRKY18 and WRKY53 coordinate with HISTONE ACETYLTRANSFERASE1 to regulate rapid responses to sugar. Plant Physiol. **180**:2212–2226.

Hao, Y., Wang, H., Qiao, S., Leng, L., and Wang, X. (2016). Histone deacetylase HDA6 enhances brassinosteroid signaling by inhibiting the BIN2 kinase. Proc. Natl. Acad. Sci. U S A **113**:10418–10423.

Hartl, M., Füßl, M., Boersema, P.J., Jost, J.-O., Kramer, K., Bakirbas, A., Sindlinger, J., Plöchinger, M., Leister, D., Uhrig, G., et al. (2017). Lysine acetylome profiling uncovers novel histone deacetylase substrate proteins in *Arabidopsis*. Mol. Syst. Biol. **13**:949.

Hellemans, J., Mortier, G., De Paepe, A., Speleman, F., and Vandesompele, J. (2007). qBase relative quantification framework and software for management and automated analysis of real-time quantitative PCR data. Genome Biol. **8**:R19.

Hinderhofer, K., and Zentgraf, U. (2001). Identification of a transcription factor specifically expressed at the onset of leaf senescence. Planta **213**:469–473.

Hu, Y., Lu, Y., Zhao, Y., and Zhou, D.-X. (2019). Histone acetylation dynamics integrates metabolic activity to regulate plant response to stress. Front. Plant Sci. **10**:1236.

Ingram, J., and Bartels, D. (1996). The molecular basis of dehydration tolerance in plants. Annu. Rev. Plant Biol. **47**:377–403.

Jeandroz, S., and Lamotte, O. (2017). Plant responses to biotic and abiotic stresses: lessons from cell signaling. Front. Plant Sci. **8**:1772.

Kang, M.J., Jin, H.S., Noh, Y.S., and Noh, B. (2015). Repression of flowering under a noninductive photoperiod by the HDA9-AGL19-FT module in *Arabidopsis*. New Phytol. **206**:281–294.

Kawashima, T., and Berger, F. (2014). Epigenetic reprogramming in plant sexual reproduction. Nat. Rev. Genet. **15**:613–624.

Kim, K.C., Lai, Z., Fan, B., and Chen, Z. (2008). Arabidopsis WRKY38 and WRKY62 transcription factors interact with histone deacetylase 19 in basal defense. Plant Cell **20**:2357–2371.

Kim, W., Latrasse, D., Servet, C., and Zhou, D.-X. (2013). *Arabidopsis* histone deacetylase HDA9 regulates flowering time through repression of AGL19. Biochem. Biophys. Res. Commun. **432**:394–398.

Kim, Y.J., Wang, R., Gao, L., Li, D., Xu, C., Mang, H., Jeon, J., Chen, X., Zhong, X., and Kwak, J.M. (2016). POWERDRESS and HDA9 interact and promote histone H3 deacetylation at specific genomic sites in *Arabidopsis*. Proc. Natl. Acad. Sci. U S A **113**:14858–14863.

Kim, J.-M., To, T.K., Matsui, A., Tanoi, K., Kobayashi, N.I., Matsuda, F., Habu, Y., Ogawa, D., Sakamoto, T., and Matsunaga, S. (2017). Acetate-mediated novel survival strategy against drought in plants. Nat. Plants **3**:17097.

Lachner, M., Sengupta, R., Schotta, G., and Jenuwein, T. (2004). Trilogies of histone lysine methylation as epigenetic landmarks of the eukaryotic genome. Cold Spring Harb. Symp. Quant. Biol. **69**:209–218.

Li, X., Wang, X., He, K., Ma, Y., Su, N., He, H., Stolc, V., Tongprasit, W., Jin, W., and Jiang, J. (2008). High-resolution mapping of epigenetic modifications of the rice genome uncovers interplay between DNA methylation, histone methylation, and gene expression. Plant Cell **20**:259–276.

Liu, X., Luo, M., Yang, S., and Wu, K. (2015). Role of epigenetic modifications in plant responses to environmental stresses. In Nuclear Functions in Plant Transcription, Signaling and Development, O. Pontes and H. Jin, eds. (New York: Springer), pp. 81–92.

Liu, X., Wei, W., Zhu, W., Su, L., Xiong, Z., Zhou, M., Zheng, Y., and Zhou, D.-X. (2017). Histone deacetylase AtSRT1 links metabolic flux and stress response in *Arabidopsis*. Mol. Plant **10**:1510–1522.

Lu, Y., Xu, Q., Liu, Y., Yu, Y., Cheng, Z.Y., Zhao, Y., and Zhou, D.X. (2018). Dynamics and functional interplay of histone lysine butyrylation, crotonylation, and acetylation in rice under starvation and submergence. Genome Biol. **19**:144.

Luo, M., Cheng, K., Xu, Y., Yang, S., and Wu, K. (2017). Plant responses to abiotic stress regulated by histone deacetylases. Front. Plant Sci. **8**:2147.

Miao, Y., and Zentgraf, U. (2007). The antagonist function of *Arabidopsis* WRKY53 and ESR/ESP in leaf senescence is modulated by the jasmonic and salicylic acid equilibrium. Plant Cell **19**:819–830.

Miao, Y., Laun, T., Zimmermann, P., and Zentgraf, U. (2004). Targets of the WRKY53 transcription factor and its role during leaf senescence in *Arabidopsis*. Plant Mol. Biol. **55**:853–867.

Miao, Y., Laun, T.M., Smykowski, A., and Zentgraf, U. (2007). *Arabidopsis* MEKK1 can take a short cut: it can directly interact with senescence-related WRKY53 transcription factor on the protein level and can bind to its promoter. Plant Mol. Biol. **65**:63–76.

Mikkelsen, T.S., Ku, M., Jaffe, D.B., Issac, B., Lieberman, E., Giannoukos, G., Alvarez, P., Brockman, W., Kim, T.-K., and Koche, R.P. (2007). Genome-wide maps of chromatin state in pluripotent and lineage-committed cells. Nature **448**:553–560.

Murray, S.L., Ingle, R.A., Petersen, L.N., and Denby, K.J. (2007). Basal resistance against Pseudomonas syringae in *Arabidopsis* involves WRKY53 and a protein with homology to a nematode resistance protein. Mol. Plant Microbe Interact. **20**:1431–1438.

Pandey, R., MuÈller, A., Napoli, C.A., Selinger, D.A., Pikaard, C.S., Richards, E.J., Bender, J., Mount, D.W., and Jorgensen, R.A. (2002). Analysis of histone acetyltransferase and histone deacetylase families of *Arabidopsis thaliana* suggests functional diversification of chromatin modification among multicellular eukaryotes. Nucleic Acids Res. **30**:5036–5055.

Ruijter, J.M., Ramakers, C., Hoogaars, W.M., Karlen, Y., Bakker, O., van den Hoff, M.J., and Moorman, A.F. (2009). Amplification efficiency: linking baseline and bias in the analysis of quantitative PCR data. Nucleic Acids Res. **37**:e45.

Sarris, P.F., Duxbury, Z., Huh, S.U., Ma, Y., Segonzac, C., Sklenar, J., Derbyshire, P., Cevik, V., Rallapalli, G., and Saucet, S.B. (2015). A plant immune receptor detects pathogen effectors that target WRKY transcription factors. Cell **161**:1089–1100.

Sarwat, M. (2017). Leaf senescence in plants: nutrient remobilization and gene regulation. In Stress Signaling in Plants: Genomics and Proteomics Perspective, *vol. 2*, M. Sarwat, A. Ahmad, M.Z. Abdin, and M.M. Ibrahim, eds. (New York: Springer), pp. 301–316.

Schütze, K., Harter, K., and Chaban, C. (2009). Bimolecular fluorescence complementation (BiFC) to study protein-protein interactions in living plant cells. Methods Mol. Biol. **479**:189–202.

Schledzewski, K., and Mendel, R.R. (1994). Quantitative transient gene expression: comparison of the promoters for maize polyubiquitin1, rice actin1, maize-derivedEmu andCaMV 35S in cells of barley, maize and tobacco. Transgenic Res. **3**:249–255.

Shen, Y., Wei, W., and Zhou, D.-X. (2015). Histone acetylation enzymes coordinate metabolism and gene expression. Trends Plant Sci. **20**:614–621.

Shen, Y., Lei, T., Cui, X., Liu, X., Zhou, S., Zheng, Y., Guérard, F., Issakidis-Bourguet, E., and Zhou, D.-X. (2019). *Arabidopsis* histone deacetylase HDA15 directly represses plant response to elevated ambient temperature. Plant J. **100**:991–1006.

Shinozaki, K., Yamaguchi-Shinozaki, K., and Seki, M. (2003). Regulatory network of gene expression in the drought and cold stress responses. Curr. Opin. Plant Biol. **6**:410–417.

Song, C.-P., Agarwal, M., Ohta, M., Guo, Y., Halfter, U., Wang, P., and Zhu, J.-K. (2005). Role of an *Arabidopsis* AP2/EREBP-type transcriptional repressor in abscisic acid and drought stress responses. Plant Cell **17**:2384–2396.

Sun, Y., and Yu, D. (2015). Activated expression of AtWRKY53 negatively regulates drought tolerance by mediating stomatal movement. Plant Cell Rep. **34**:1295–1306.

Verdin, E., and Ott, M. (2015). 50 years of protein acetylation: from gene regulation to epigenetics, metabolism and beyond. Nat. Rev. Mol. Cell Biol. **16**:258–264.

Verslues, P.E., Agarwal, M., Katiyar-Agarwal, S., Zhu, J., and Zhu, J.K. (2006). Methods and concepts in quantifying resistance to drought, salt and freezing, abiotic stresses that affect plant water status. Plant J. **45**:523–539.

Wang, Z., Cao, H., Sun, Y., Li, X., Chen, F., Carles, A., Li, Y., Ding, M., Zhang, C., and Deng, X. (2013). Arabidopsis paired amphipathic helix proteins SNL1 and SNL2 redundantly regulate primary seed dormancy via abscisic acid–ethylene antagonism mediated by histone deacetylation. Plant Cell **25**:149–166.

Xiong, L., Schumaker, K.S., and Zhu, J.-K. (2002). Cell signaling during cold, drought, and salt stress. Plant Cell **14**:S165–S183.

Yoo, S.-D., Cho, Y.-H., and Sheen, J. (2007). *Arabidopsis* mesophyll protoplasts: a versatile cell system for transient gene expression analysis. Nat. Protoc. **2**:1565–1572.

Zanten, M., Zöll, C., Wang, Z., Philipp, C., Carles, A., Li, Y., Kornet, N.G., Liu, Y., and Soppe, W.J. (2014). HISTONE DEACETYLASE 9 represses seedling traits in *Arabidopsis thaliana* dry seeds. Plant J. **80**:475–488.

Zentgraf, U., Laun, T., and Miao, Y. (2010). The complex regulation of WRKY53 during leaf senescence of *Arabidopsis thaliana*. Eur. J. Cell Biol. **89**:133–137.

Zhang, W., Qin, C., Zhao, J., and Wang, X. (2004). Phospholipase Dα1-derived phosphatidic acid interacts with ABI1 phosphatase 2C and regulates abscisic acid signaling. Proc. Natl. Acad. Sci. U S A **101**:9508–9513.

Zhang, H., Zhao, Y., and Zhou, D.-X. (2017). Rice NAD+-dependent histone deacetylase OsSRT1 represses glycolysis and regulates the moonlighting function of GAPDH as a transcriptional activator of glycolytic genes. Nucleic Acids Res. **45**:12241–12255.

Zheng, Y., Ding, Y., Sun, X., Xie, S., Wang, D., Liu, X., Su, L., Wei, W., Pan, L., and Zhou, D.-X. (2016). Histone deacetylase HDA9 negatively regulates salt and drought stress responsiveness in *Arabidopsis*. J. Exp. Bot. **67**:1703–1713.

Zhu, J.-K. (2002). Salt and drought stress signal transduction in plants. Annu. Rev. Plant Biol. **53**:247–273.